Supporting Information

Edge-Effect Enhanced Catalytic CO Oxidation by Atomically Dispersed Pt on Nitride-Graphene

Chuanyi Jia [a],[‡] Xijun Wang [b],[‡] Huabing Yin [c],[‡] Wenhui Zhong [a], Edward Sharman [d], Yi Luo [b] and Jun Jiang [b],*

[a]Guizhou Provincial Key Laboratory of Computational Nano-material Science, Institute of Applied Physics, Guizhou Education University, Guiyang, Guizhou, 550018, China

[b]Hefei National Laboratory for Physical Sciences at the Microscale, iChEM (Collaborative Innovation Center of Chemistry for Energy Materials), CAS Center for Excellence in Nanoscience, School of Chemistry and Materials Science, University of Science and Technology of China, Hefei, Anhui, 230026, China

[c]Institute for Computational Materials Science, School of Physics and Electronics, International Joint Research Laboratory of New Energy Materials and Devices of Henan Province, Henan University, Kaifeng 475004, China

[d]Department of Neurology, University of California, Irvine, California 92697, United States

Corresponding Author

*jiangj1@ustc.edu.cn. Phone: +86 551 63600029

[‡]C.J., X.W. and H.Y. contributed equally to this work..

1. Computational Details

DFT calculations were performed using the Vienna ab initio simulation package (VASP).[1] The Perdew, Burke and Ernzerhof (PBE) functional and the projector augmented wave (PAW) method were used to simulate geometric and electronic properties.[2-5] Long-range van der Waals (vdW) interactions were taken into consideration via the DFT-D2 correction method.[6] Geometric structures were fully relaxed until energy and forces converged to 10^{-5} eV and 0.01 eV/Å, respectively. The Brillouin zone was sampled by a $5 \times 5 \times 1$ Monkhorst-Pack k-mesh, and the kinetic energy cutoff was set to 400 eV in the plane-wave expansion.[7,8]

The graphene monolayer was modeled using a rectangular 6×6 supercell with 60 carbon atoms. The vacuum region thickness separating the slabs was set to 15 Å. The DDEC6 method, which is a refinement of the Density Derived Electrostatic and Chemical (DDEC) approach, was used to analyze charge distributions.[9,10] Many theoretical and experimental works show that this method has excellent performance in 2D/3D solid material systems, confirming that it is reliable and accurate.[11-13] The climbing image nudged elastic band (CI-NEB) method was employed to search the transition states of the elementary steps along the O_2 activation and CO oxidation paths.[14,15]

The binding energy between the adsorbate and catalytic surface is calculated as:

$$E_b = E_{sur+ad} - E_{sur} - E_{ad}$$

where E_{sur+ad}, E_{sur}, and E_{ad} represent the energies of the adsorption system, the bare surface, and the free adsorbant molecules, respectively.

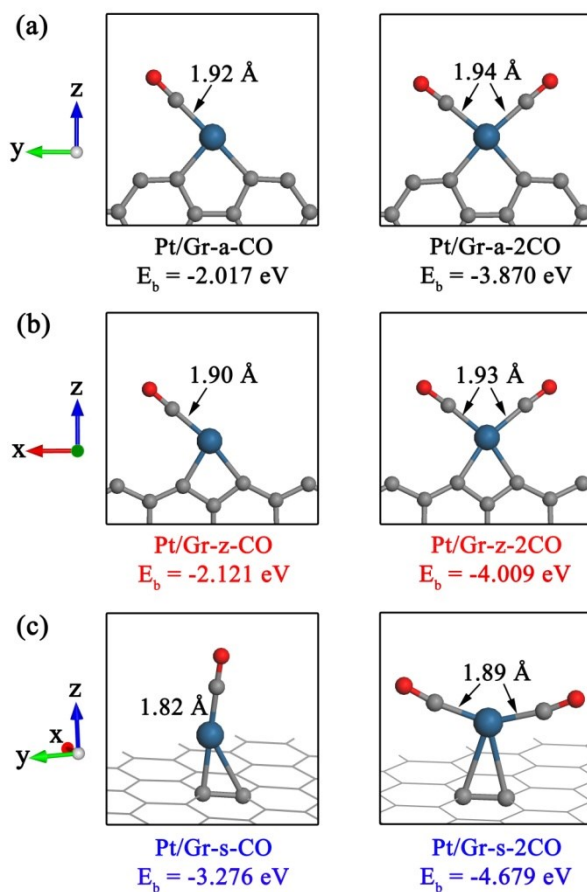## 2. Optimized Structures and Binding Energies of CO and 2CO on Pt/Gr and Pt/NGr.

Figure S1. The optimized structures and binding energies of CO and 2CO on **Pt/Gr-a (a)**, **Pt/Gr-z (b)** and **Pt/Gr-s (c)** surfaces. Dark blue, gray and red spheres represent Pt, C and O atoms, respectively.
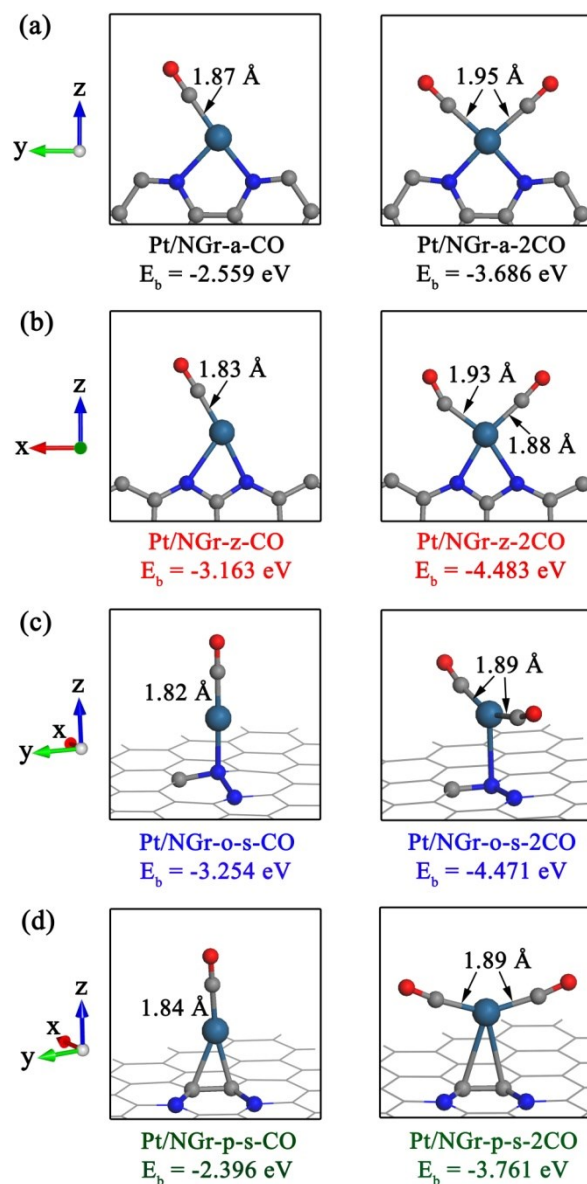
Figure S2. The optimized structures and binding energies of CO and 2CO on **Pt/NGr-a (a)**, **Pt/NGr-z (b)**, **Pt/NGr-o-s (c)** and **Pt/NGr-p-s (d)** surfaces. Blue spheres: N atoms; other atoms are colored the same as in Figure S1.

3. Optimized Structures and Relative Energies (E_{re}) of the States Identified in Figure 3. The E_{re} of the initial state (IS) are all set to 0 eV. $E_{re} = E_{TS/FS} - E_{IS}$

Figure S3. The optimized structures and relative energies of the initial (I), transition (T) and final (F) states for O_2 activation on **Pt/Gr-a (a)**, **Pt/Gr-z (b)** and **Pt/Gr-s (c)** surfaces (Figure 3a). See the Figure S1 legend for color coding.
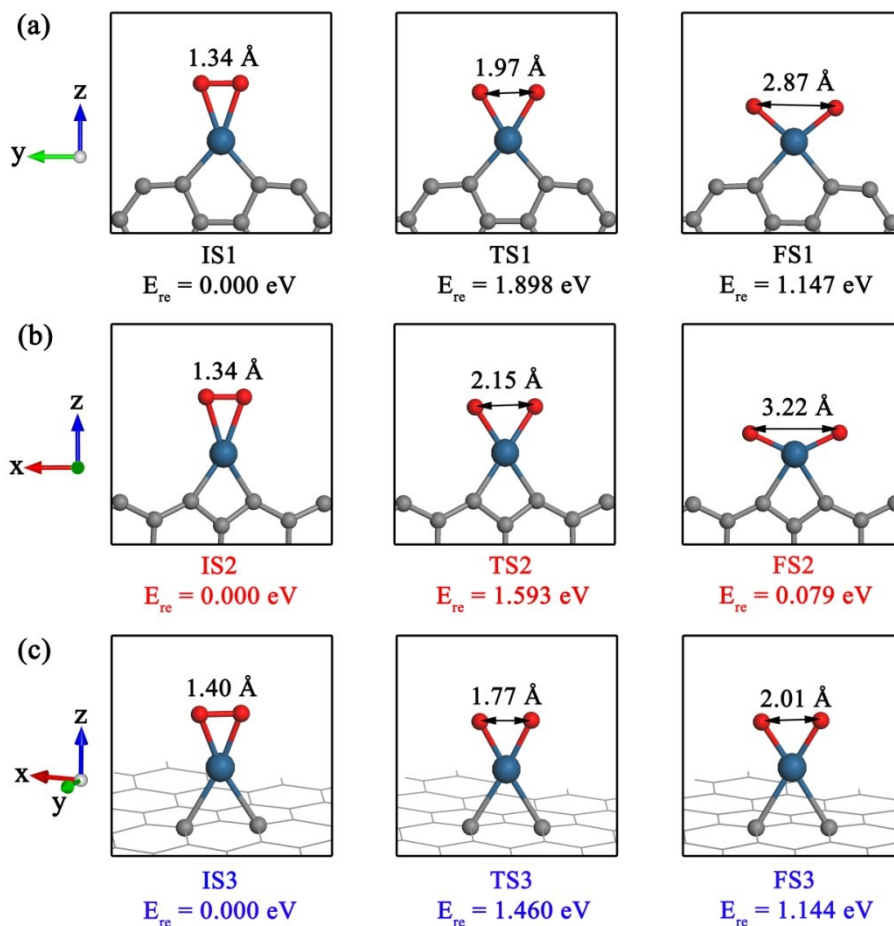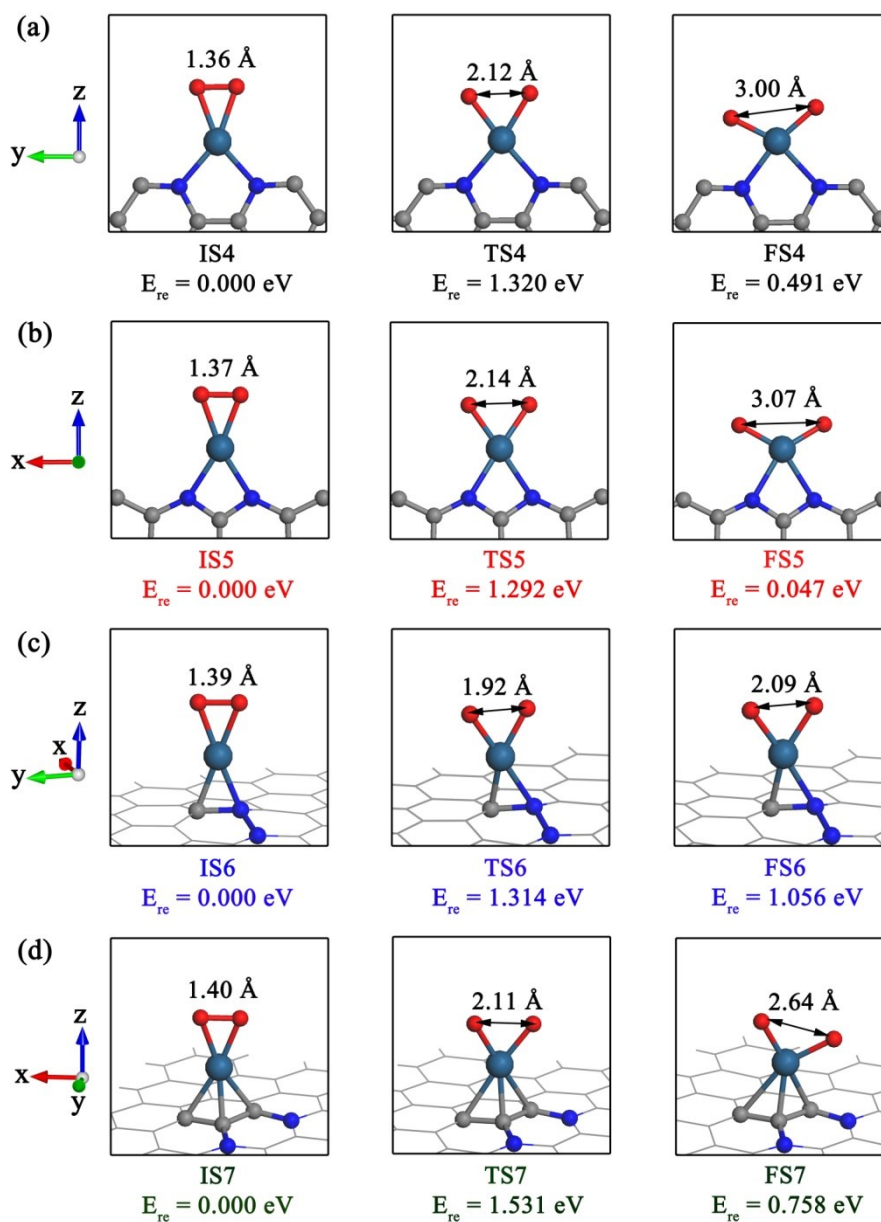
Figure S4. Optimized structures and relative energies of the initial (I), transition (T) and final (F) states for O_2 activation on **Pt/NGr-a (a)**, **Pt/NGr-z (b)**, **Pt/NGr-o-s (c)** and **Pt/NGr-p-s (d)** surfaces (Figure 3b). See the Figure S2 legend for color coding.

.

Figure S5. Optimized structures and relative energies of the initial (I), transition (T) and final (F) states for the CO+O_2 reaction on **Pt/Gr-a (a)**, **Pt/Gr-z (b)** and **Pt/Gr-s (c)** surfaces (Figure 3c). See the Figure S1 legend for color coding.

Figure S6. Optimized structures and relative energies of the initial (I), transition (T) and final (F) states for CO+O$_2$ reaction on **Pt/NGr-a (a)**, **Pt/NGr-z (b)**, **Pt/NGr-o-s (c)** and **Pt/NGr-p-s (d)** surfaces (Figure 3d). See the Figure S2 legend for color cording.

Figure S7. Optimized structures and relative energies of the initial (I), transition (T) and final (F) states for the CO+O reaction on **Pt/Gr-a (a)**, **Pt/Gr-z (b)** and **Pt/Gr-s (c)** surfaces (Figure 3e). See the Figure S1 legend for color coding.
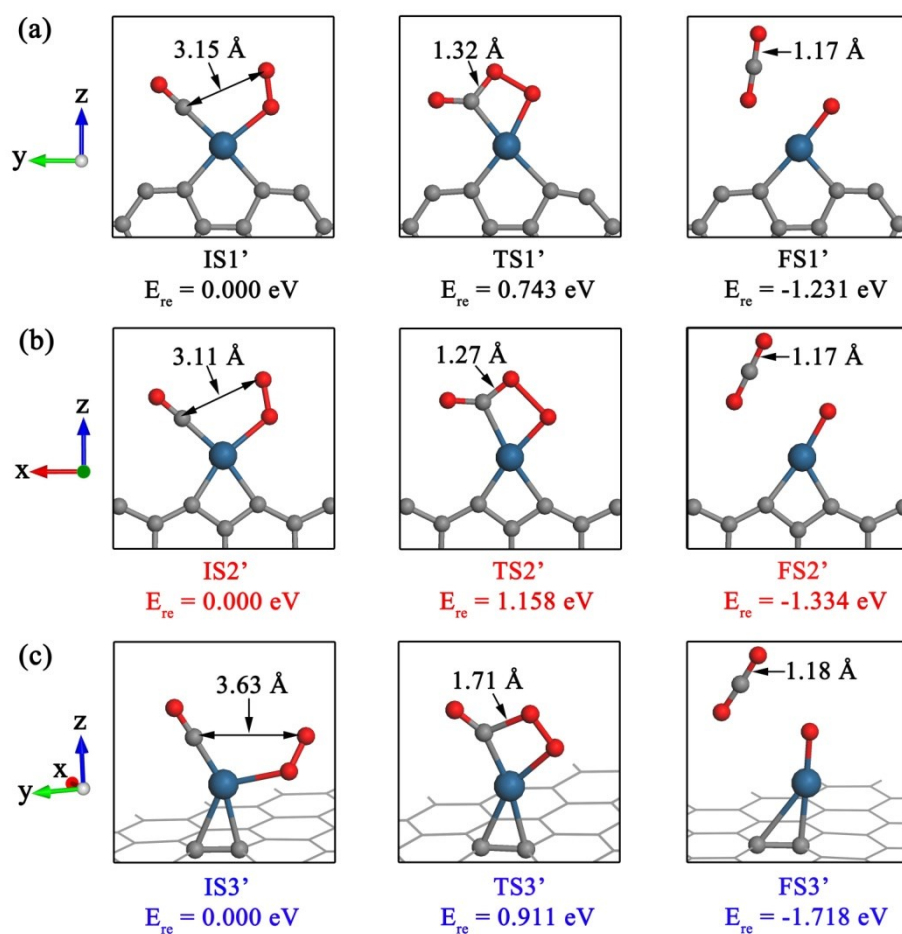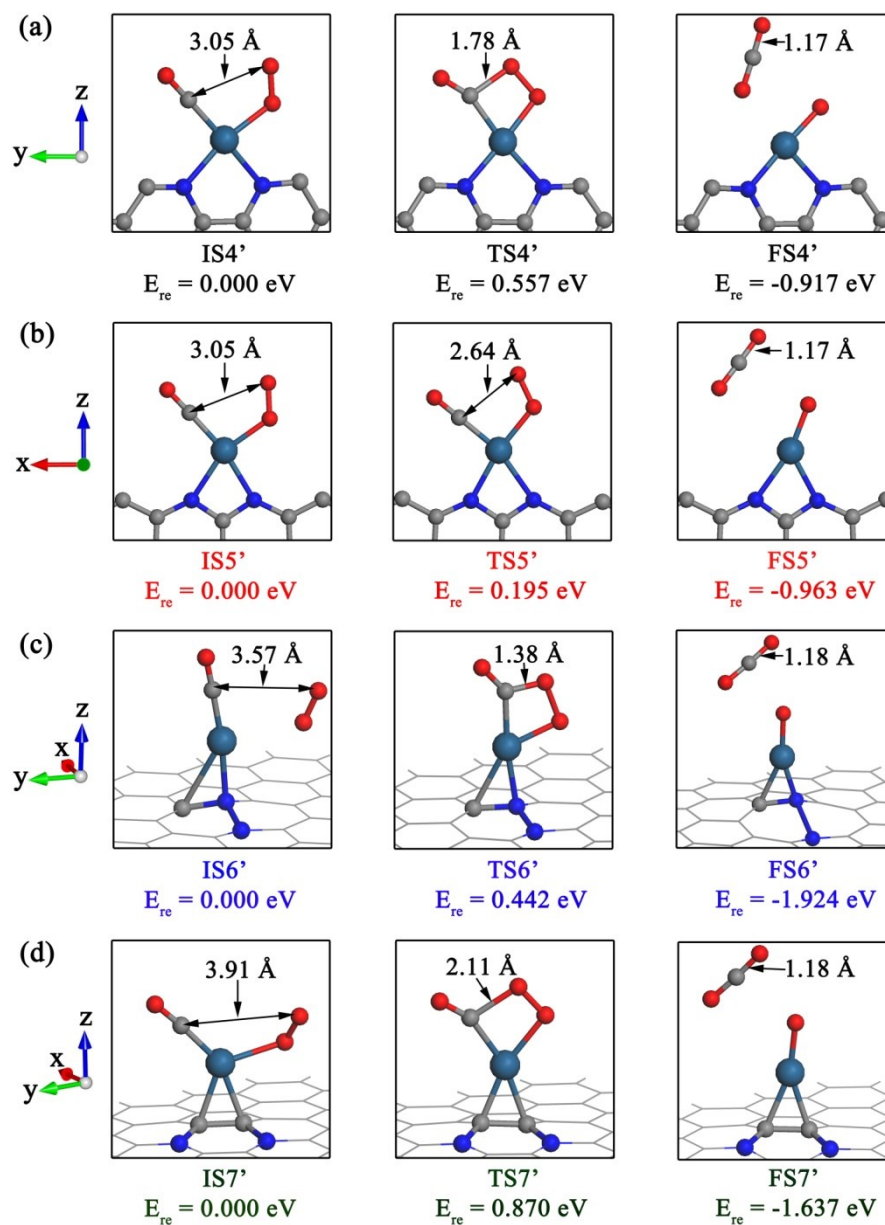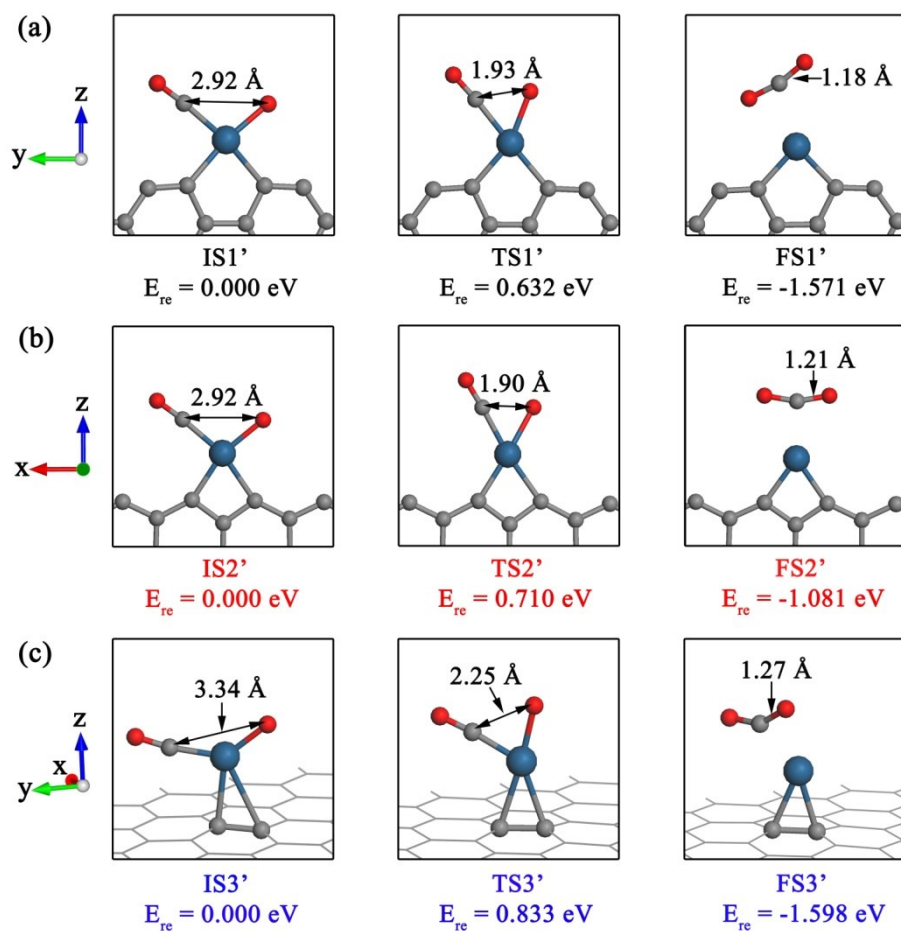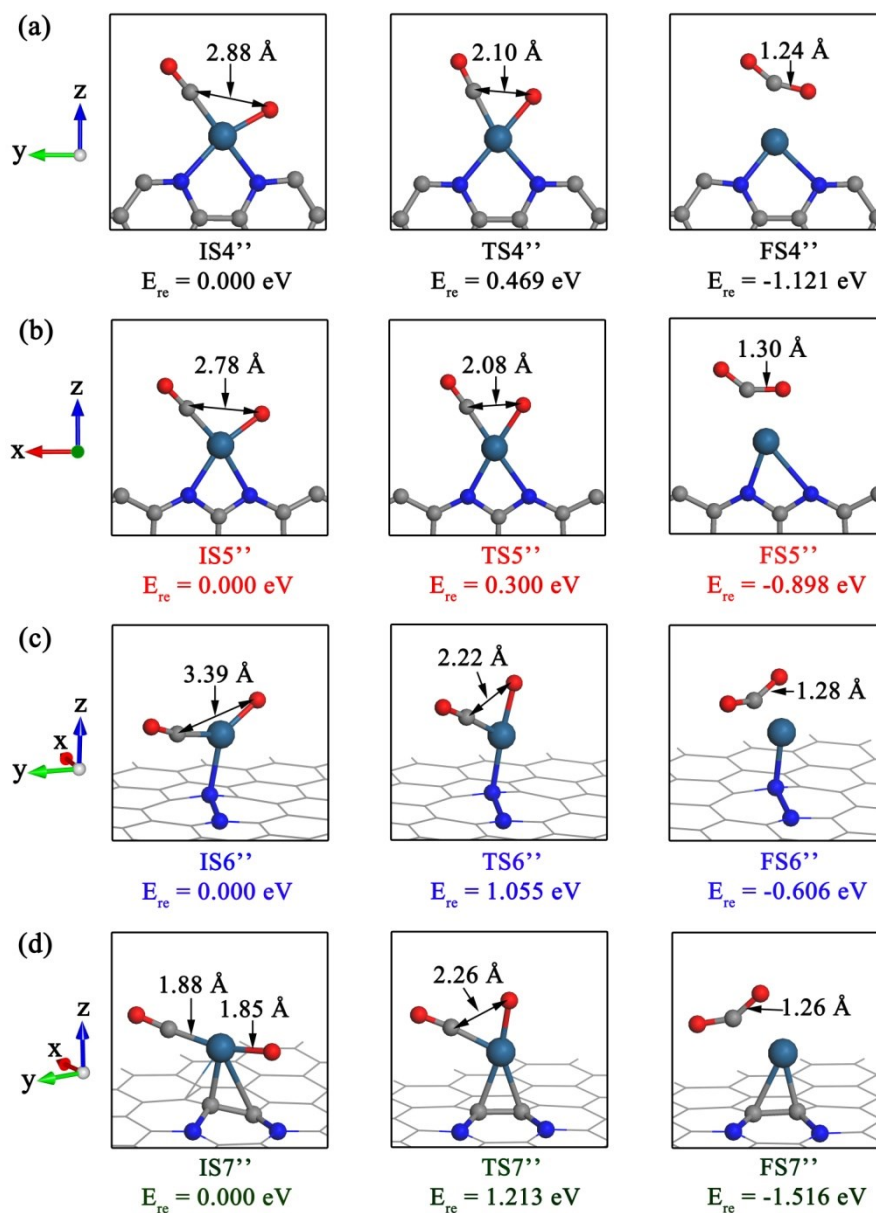
Figure S8. Optimized structures and relative energies of the initial (I), transition (T) and final (F) states for the CO+O reaction on **Pt/NGr-a (a)**, **Pt/NGr-z (b)**, **Pt/NGr-o-s (c)** and **Pt/NGr-p-s (d)** surfaces (Figure 3f). See the Figure S2 legend for color coding.

4. The Convergence Test for the Embedded Model of Pt on NGr.

The calculation results for the embedded model of Pt on NGr (denoted as Pt/NGr-e) indicate that since the adsorbed O_2 molecule is too close to the surface N atoms, the large repulsive forces between them jeopardize the stable adsorption of O_2/CO+O_2 on the Pt site (the O_2 is more inclined to stay far away from the surface). Thus, the embedded model of Pt on NGr is not suitable for O_2 activation and CO oxidation investigations.
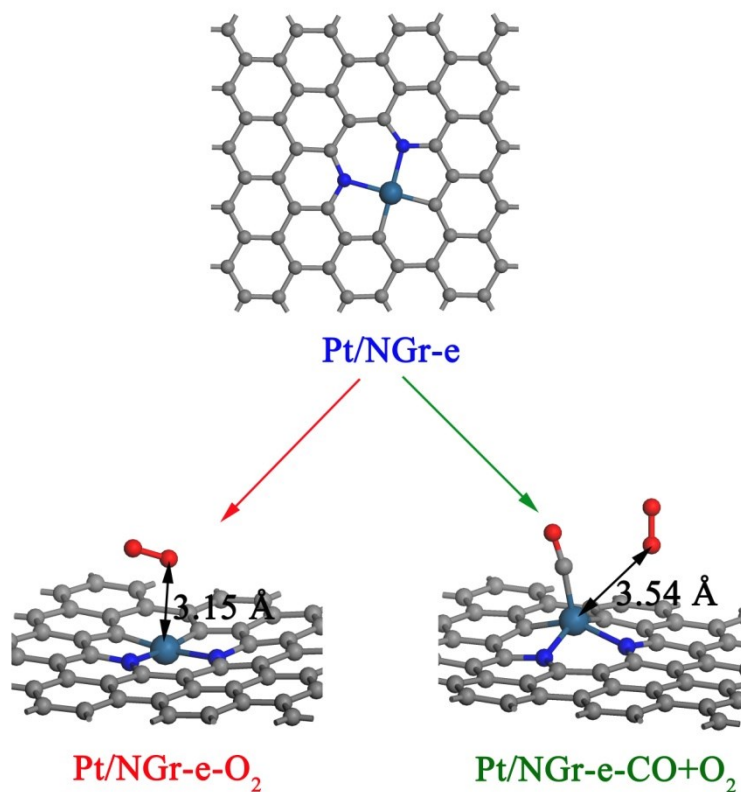
Figure S9. The optimized structure of the embedded model of Pt on NGr (Pt/NGr-e) and corresponding binding structures of O_2 and CO+O_2 on the single Pt atoms. See the Figure S2 legend for color coding.

5. Optimized Binding Structures and Corresponding Electronic Properties of the Pt/NGr Configurations.
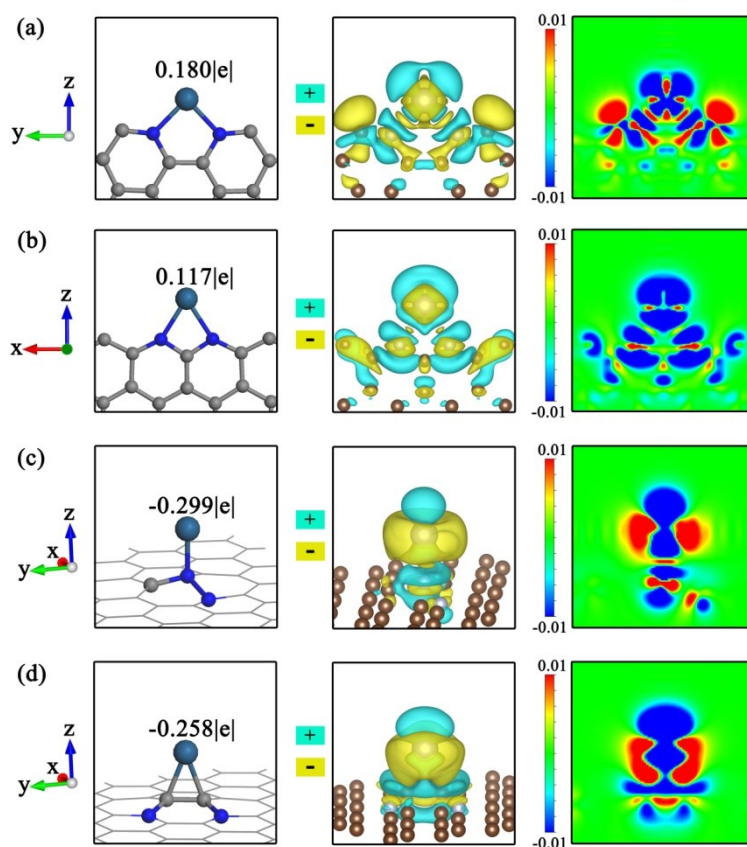
Figure S10. Optimized binding structures and corresponding electronic properties of the **Pt/NGr-a (a)**, **Pt/NGr-z (b)**, **Pt/NGr-o-s (c)** and **Pt/NGr-p-s (d)** configurations. **Left:** Binding structures and DDEC (density derived electrostatic and chemical) charges of Pt atoms; **Middle:** three-dimensional differential charge density maps; **Right:** two-dimensional differential charge density maps. The detailed charge density distribution is shown in Figure S12.

(a)

1: 0.205   2: -0.018   3: -0.147
4: -0.145   5: -0.019   6: 0.013
7: 0.044   8: 0.043   9: 0.013
10: 0.013   11: 0.009   12: 0.010
13: 0.012

(b)

1: 0.156   2: -0.034   3: 0.019
4: -0.097   5: 0.017   6: -0.097
7: 0.018   8: -0.035   9: -0.007
10: 0.026   11: -0.001   12: 0.030
13: -0.002 14: 0.026   15: -0.007

(c)

1: -0.060   2: 0.014   3: 0.002   4: -0.002
5: 0.002   6: -0.002   7: 0.000   8: 0.000
9: -0.004   10: 0.002   11: 0.001   12: -0.001
13: 0.000   14: 0.000   15: -0.005 16: 0.000
17: 0.014

Figure S11. Optimized binding structures (**Left**) and corresponding charge ($|e|$) density distribution (**Right**) of the **Pt/Gr-a (a)**, **Pt/Gr-z (b)** and **Pt/Gr-s (c)** configurations.

(a)

1: 0.180   2: -0.162   3: -0.100
4: -0.102   5: -0.161   6: 0.023
7: 0.104   8: 0.107   9: 0.024
10: 0.028   11: -0.009   12: -0.009
13: 0.027

(b)

1: 0.117   2: -0.091   3: 0.157
4: -0.264   5: 0.308   6: -0.263
7: 0.158   8: -0.093   9: 0.007
10: -0.025 11: 0.029   12: -0.062
13: 0.028   14: -0.023   15: 0.006

(c)

1: -0.299   2: 0.060   3: -0.022   4: 0.014
5: 0.001   6: 0.014   7: -0.022   8: -0.044
9: 0.092   10: -0.029 11: 0.091   12: -0.047
13: -0.021   14: 0.061   15: -0.023 16: -0.001
17: 0.115

(d)

1: -0.258   2: 0.088   3: -0.028   4: 0.014
5: -0.056   6: 0.120   7: -0.043   8: 0.057
9: 0.058   10: -0.044 11: 0.121   12: -0.054
13: 0.014   14: -0.029 15: 0.008   16: 0.004
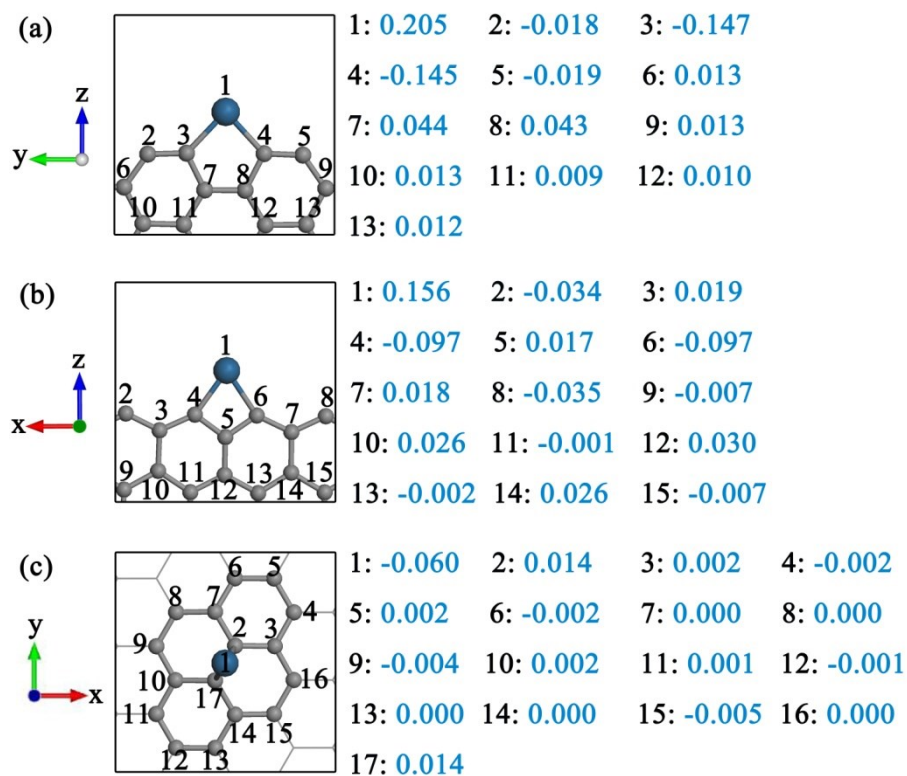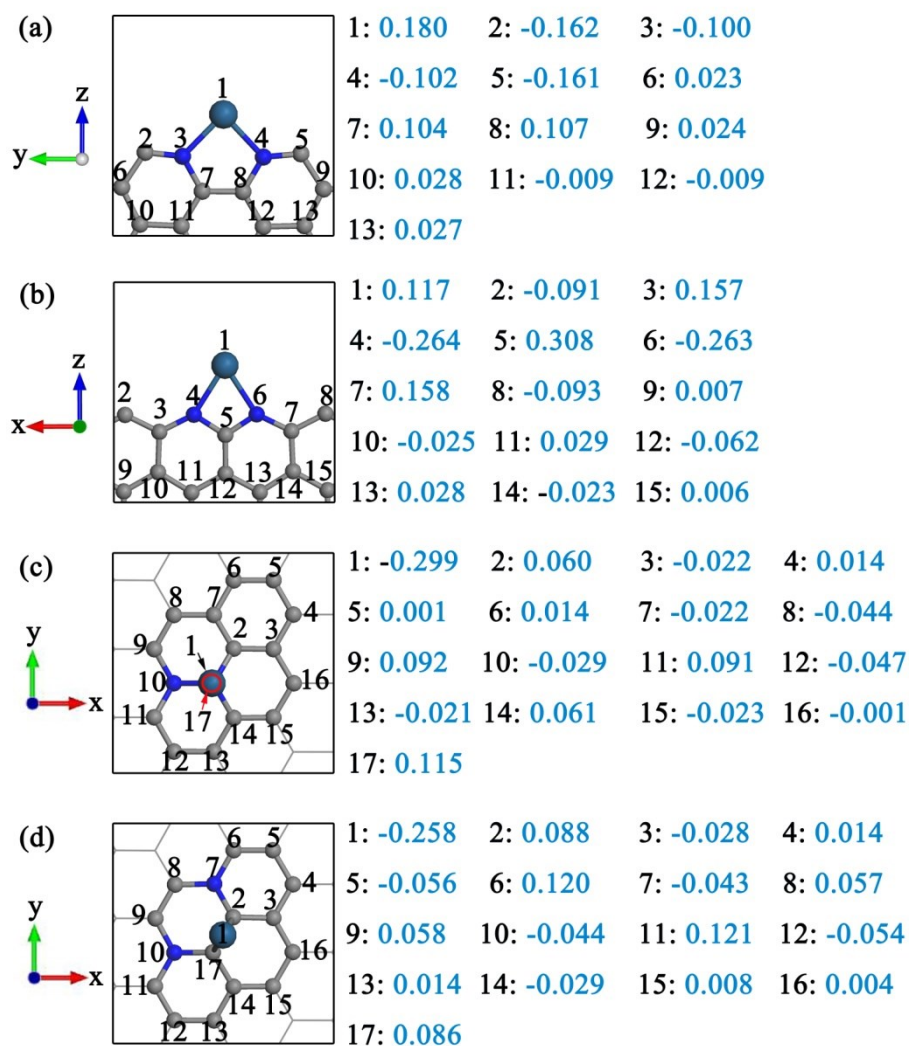17: 0.086

Figure S12. Optimized binding structures (**Left**) and corresponding charge ($|e|$) density distribution (**Right**) of the **Pt/NGr-a (a)**, **Pt/NGr-z (b)**, **Pt/NGr-o-s (c)** and **Pt/NGr-p-s (d)** configurations.

6. Detailed Charge, Binding Energy and Energy Barrier Values for O_2 Activation, and the CO+O_2 and CO+O Reaction Steps.

Table S1. Calculated Pt and adsorbate (*ads*) charges after O_2, CO+O_2 and CO+O adsorption; the corresponding binding energies (E_b) and energy barriers for O_2 activation, and the CO+O_2 and CO+O reaction steps. Bold data: energy barrier of the rate-determining step for CO oxidation.

	Pt/Gr-	Pt/Gr-	Pt/Gr-	Pt/NGr-	Pt/NGr-	Pt/NGr-o-	Pt/NGr-p-
Pt-Charge(O_2)/|e|	0.180	0.090	0.199	0.231	0.252	0.071	0.126
ads-Charge(O_2)/|e|	-0.160	-0.163	-0.333	-0.178	-0.204	-0.320	-0.360
$E_b(O_2)$/eV	-1.056	-1.608	-1.555	-1.650	-2.854	-1.848	-1.049
Energy Barrier/eV	1.898	1.593	1.460	1.320	1.292	1.314	1.531
Pt-Charge(CO+O_2)/|e|	0.144	0.110	-0.018	0.207	0.265	-0.250	-0.059
ads-Charge(CO+O_2)/|e|	-0.022	-0.091	-0.144	-0.083	-0.133	-0.039	-0.216
$E_b(CO+O_2)$/eV	-2.649	-2.850	-3.119	-3.079	-4.303	-3.401	-2.823
Energy Barrier/eV	**0.743**	**1.158**	**0.911**	**0.557**	0.195	0.442	0.870
Pt-Charge(CO+O)/|e|	0.257	0.194	0.179	0.297	0.450	0.128	0.080
ads-Charge(CO+O)/|e|	-0.130	-0.220	-0.441	-0.356	-0.337	-0.503	-0.610
$E_b(CO+O)$/eV	-1.861	-2.367	-2.883	-2.511	-3.760	-3.352	-3.122
Energy Barrier/eV	0.632	0.710	0.833	0.469	**0.300**	**1.055**	**1.213**

For CO + O_2 adsorption on Pt/NGr-o-s, because of the large repulsive force of the adsorbed CO, the O_2 molecule cannot form a Pt-O bond with the surface Pt atom, as shown in Figure S6. Thus, electron transfer between the adsorbates (CO+O_2) and Pt/NGr-o-s is much lower than in other configurations, making this a special state that does not follow the same rule as other states (sharp-tip electron-aggregation effect).

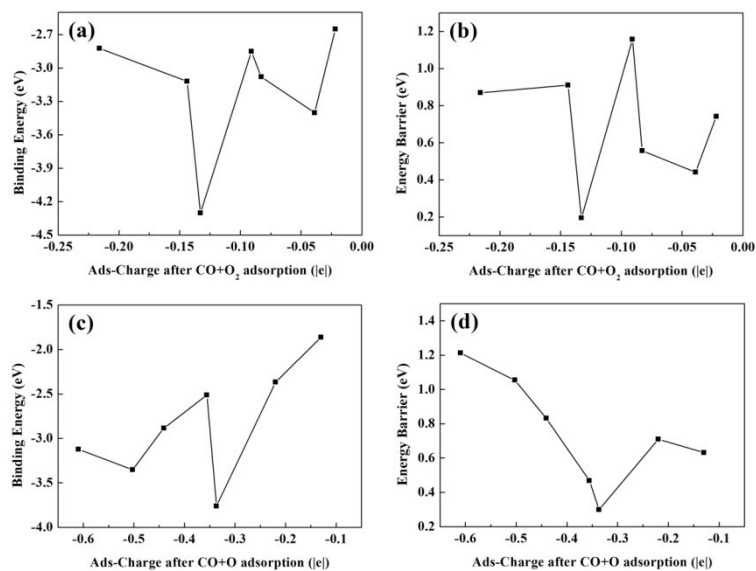# 7. Correlations between the Polarization Charge of Reactants ($CO+O_2$/$CO+O$) and Their Stability/Reactivity.

Figure S13. Correlations for the reactant ($CO+O_2$/$CO+O$) polarization charge and its stability/reactivity. **Ads:** adsorbed reactant. Detailed charge and energy values are shown in Table S1.

8. The Diffusion Behaviors of Pt-SACs on Gr/NGr Supports.

From Figure S14, we note that the edge-path is much more favorable than center-path. Thus, we only test the different edge-paths (edge-N-path and edge-C-path) on NGr surfaces, as shown in Figure S14.

Figure S14. Optimized structures and binding (E_b) and relative (E_{re}) energies of the initial (I), transition (T) and final (F) states for Pt-diffusion reactions on **Pt/Gr-a (a)**, **Pt/Gr-z (b)** and **Pt/Gr-s ((c)** and **(d)**) surfaces. **Pt/Gr-s-XX(c):** the center-path on the Gr surface; **Pt/Gr-s-XX(e):** the edge-path on the Gr surface. Red arrow: the diffusion path of single Pt atom. See the Figure S1 legend for color coding.

(a)

Pt/NGr-a-IS
E_b = -4.301 eV
E_{re} = 0.000 eV

Pt/NGr-a-TS
E_b = -3.393 eV
E_{re} = 0.908 eV

Pt/NGr-a-FS
E_b = -6.379 eV
E_{re} = -2.078 eV

2.01 Å   1.89 Å   1.99 Å

(b)

Pt/NGr-z-IS
E_b = -3.343 eV
E_{re} = 0.000 eV

Pt/NGr-z-TS
E_b = -2.824 eV
E_{re} = 0.519 eV

Pt/NGr-z-FS
E_b = -5.129 eV
E_{re} = -1.786 eV

2.12 Å   1.96 Å   2.40 Å

(c)

Pt/NGr-o-s-IS (N)
E_b = -2.671 eV
E_{re} = 0.000 eV

Pt/NGr-o-s-TS (N)
E_b = -1.588 eV
E_{re} = 1.083 eV

Pt/NGr-o-s-FS (N)
E_b = -3.350 eV
E_{re} = -0.679 eV

(d)

Pt/NGr-o-s-IS (C)
E_b = -2.671 eV
E_{re} = 0.000 eV

Pt/NGr-o-s-TS (C)
E_b = -2.469 eV
E_{re} = 0.202 eV

Pt/NGr-o-s-FS (C)
E_b = -3.350 eV
E_{re} = -0.679 eV

(e)

Pt/NGr-p-s-IS (N)
E_b = -3.590 eV
E_{re} = 0.000 eV

Pt/NGr-p-s-TS (N)
E_b = -2.135 eV
E_{re} = 1.455 eV

Pt/NGr-p-s-TS (N)
E_b = -3.590 eV
E_{re} = 0.000 eV

(f)

Pt/NGr-p-s-IS (C)
E_b = -3.590 eV
E_{re} = 0.000 eV

Pt/NGr-p-s-TS (C)
E_b = -2.367 eV
E_{re} = 0.953 eV

Pt/NGr-p-s-TS (C)
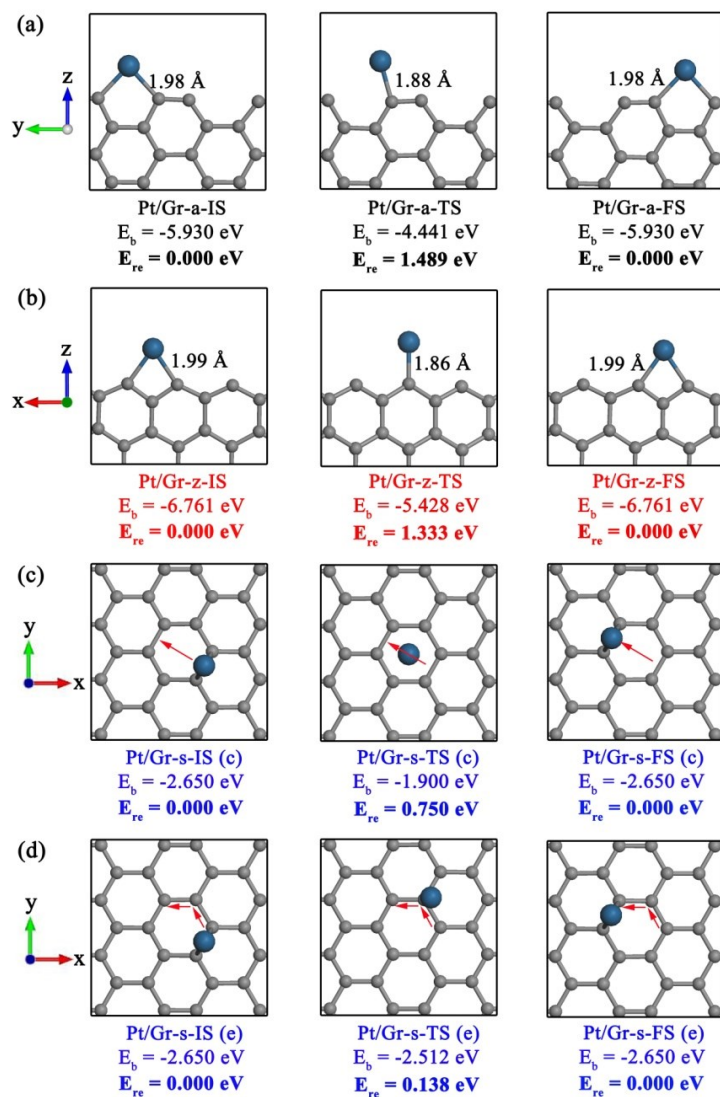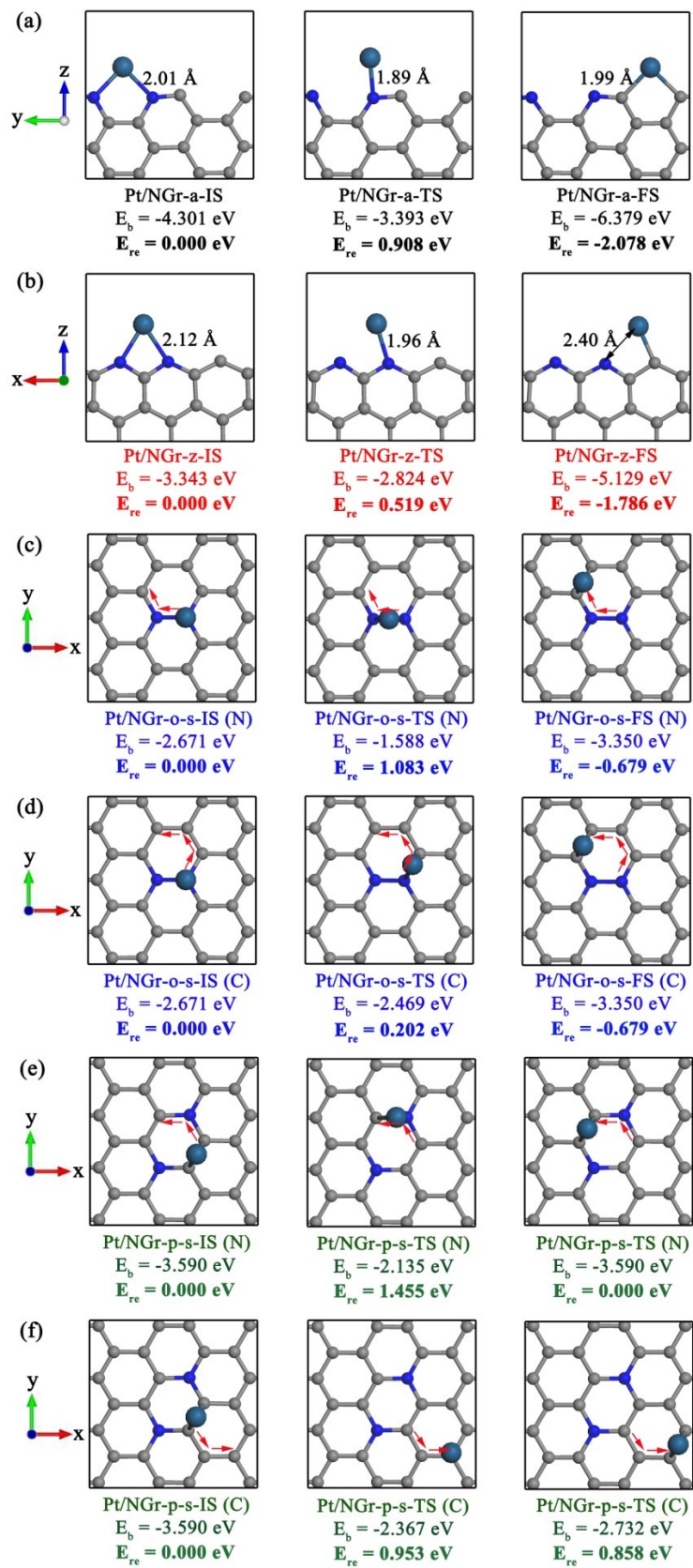E_b = -2.732 eV
E_{re} = 0.858 eV

Figure S15. Optimized structures and binding (E_b) and relative (E_{re}) energies of the initial (I), transition (T) and final (F) states for Pt-diffusion reactions on **Pt/NGr-a (a)**,

Pt/NGr-z **(b)**, **Pt/NGr-o-s** (**(c)** and **(d)**) and **Pt/NGr-p-s** (**(e)** and **(f)**) surfaces. **Pt/NGr-x-s-XX(N):** the edge-N-path on the NGr surface; **Pt/Gr-x-s-XX(C):** the edge-C-path on the NGr surface. Red arrow: the diffusion path of single Pt atom. See the Figure S2 legend for color coding.

Table S2. Calculated binding energies (E_b) and diffusion barriers (most favorable path) of Pt single atoms on Gr/NGr supports, the corresponding CO oxidation barriers (rate-determining step), and their energy differences (ΔE). $\Delta E = E(Diffusion\ Barrier) - E(CO\ oxidation\ Barrier)$. According to this definition, positive value of ΔE means a more stable active site under reaction conditions.

	Pt/Gr-a	Pt/Gr-z	Pt/Gr-s	Pt/NGr-a	Pt/NGr-z	Pt/NGr-o-s	Pt/NGr-p-s
$E_b(Pt)/eV$	-5.930	-6.761	-2.650	-4.301	-3.343	-2.671	-3.590
Diffusion Barrier/eV	1.489	1.333	0.138	0.908	0.519	0.202	0.953
CO oxidation Barrier/eV	0.743	1.158	0.911	0.557	0.300	1.055	1.213
$\Delta E/eV$	**0.746**	**0.175**	**-0.773**	**0.351**	**0.219**	**-0.853**	**-0.260**

9. The Catalytic Performances and Diffusion Behaviors of Pt-SACs on Gr/N$_1$Gr Supports.
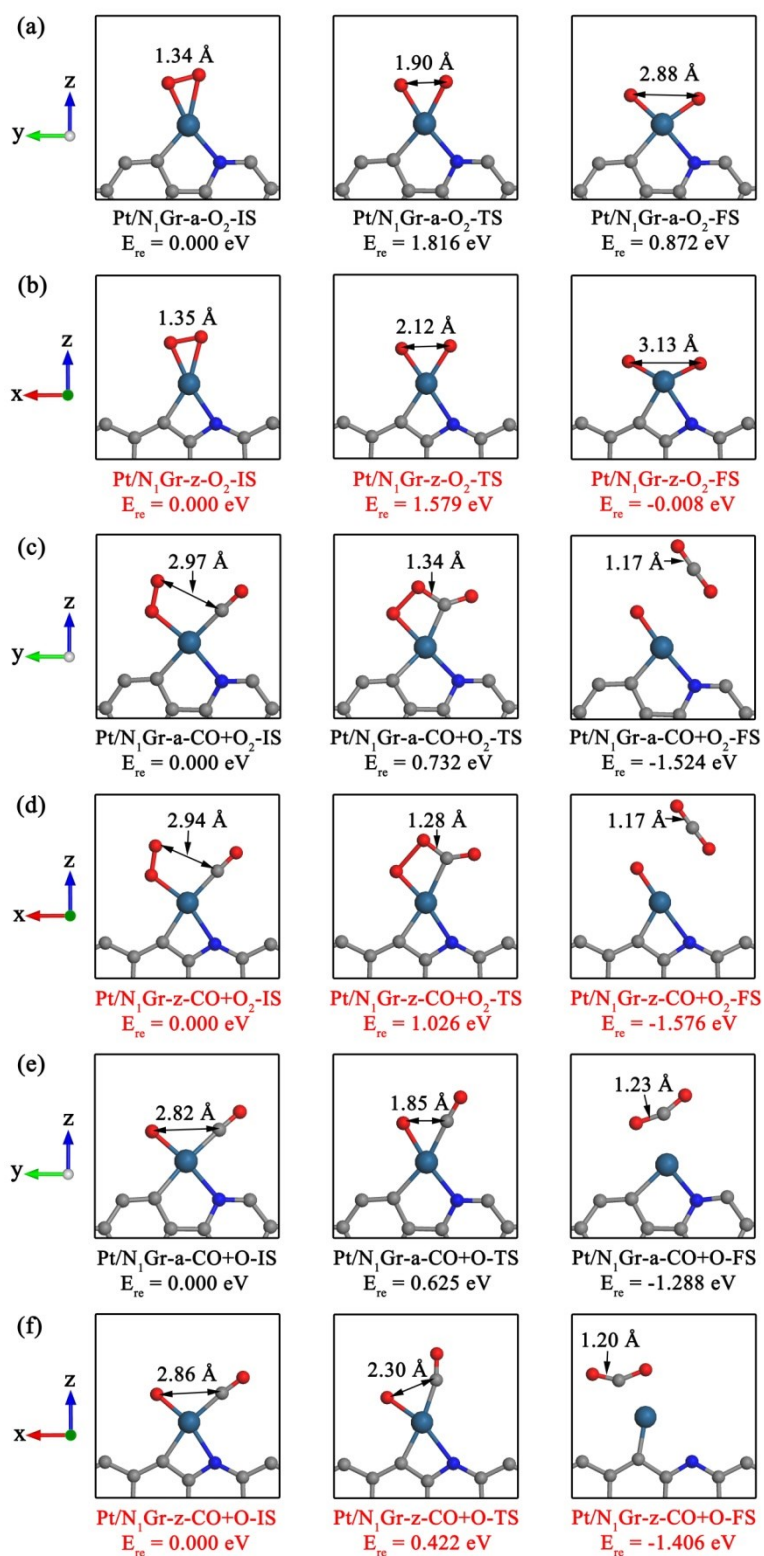

Figure S16. Optimized structures and relative energies of the initial (I), transition (T)

and final (F) states for O_2 activation (**a**, **b**), and $CO+O_2$ (**c**, **d**) and $CO+O$ (**e**, **f**) reactions on **Pt/N₁Gr-a** and **Pt/N₁Gr-z** surfaces. The detailed binding energies of the reactants are shown in Table S3. See the Figure S2 legend for color coding.
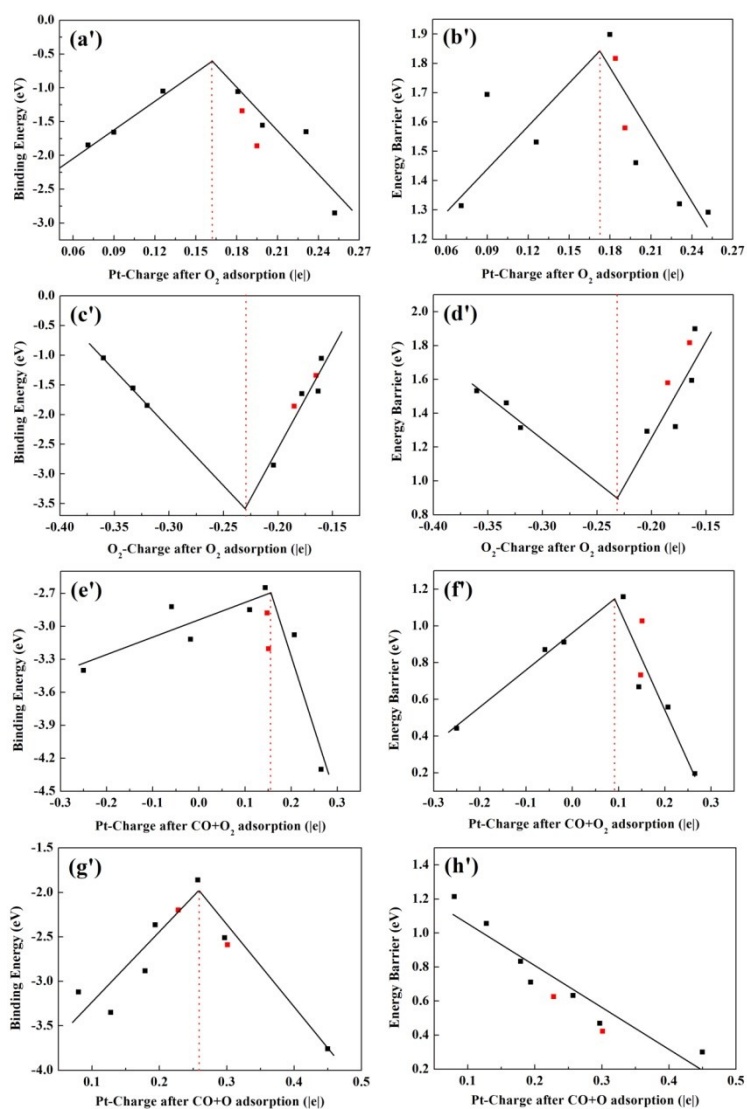

Figure S17. Correlations between the Pt/O_2 polarization charges and stability/reactivity of the reactants (O_2, $CO+O_2$ and $CO+O$). Black dots: Pt/Gr and Pt/NGr; Red dots: Pt/N₁Gr. Detailed charge and energy values are shown in Tables S1 and S3.
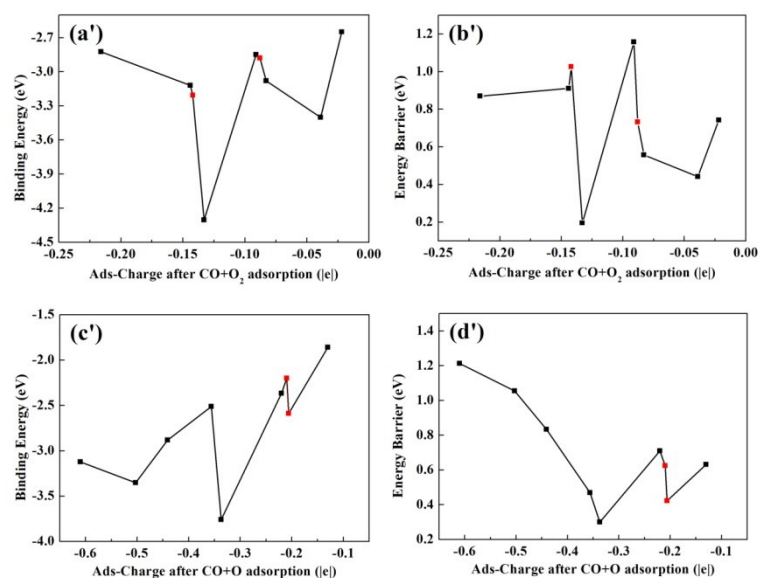
Figure S18. Correlations for the reactant ($CO+O_2$/$CO+O$) polarization charge and its stability/reactivity. **Ads:** adsorbed reactant. Black dots: Pt/Gr and Pt/NGr; Red dots: Pt/N_1Gr. Detailed charge and energy values are shown in Tables S1 and S3.
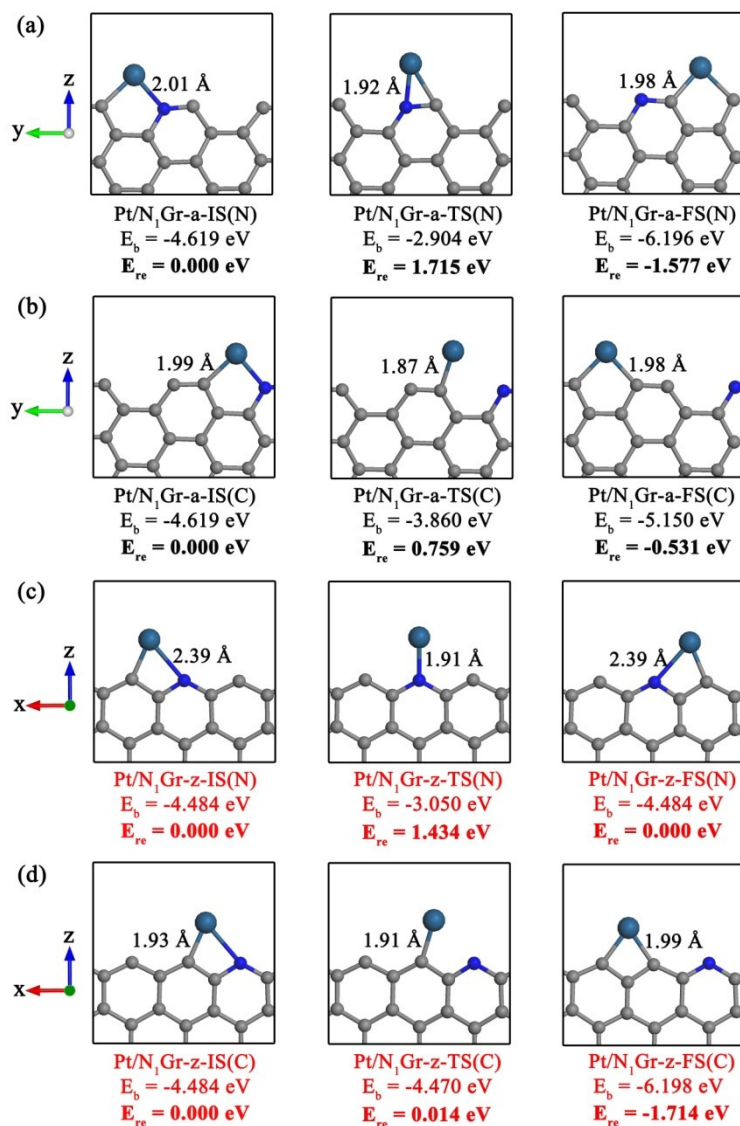
Figure S19. Optimized structures and binding (E_b) and relative (E_{re}) energies of the initial (I), transition (T) and final (F) states for Pt-diffusion reactions on **Pt/N$_1$Gr-a** (**(a)** and **(b)**) and **Pt/N$_1$Gr-z** (**(c)** and **(d)**) surfaces. **Pt/N$_1$Gr-x-XX(N):** Pt diffuses along the N side; **Pt/N$_1$Gr-x-XX(C):** Pt diffuses along the C side. See the Figure S2 legend for color coding.

Table S3. Calculated Pt and adsorbate (*ads*) charges after O_2, $CO+O_2$ and $CO+O$ adsorption on the edges of Pt/Gr, Pt/N_1Gr and Pt/NGr catalysts; the corresponding binding energies (E_b) and energy barriers for O_2 activation, and the $CO+O_2$ and $CO+O$ reaction steps.

	Pt/Gr-	Pt/N₁Gr-	Pt/NGr-	Pt/Gr-	Pt/N₁Gr-	Pt/NGr-
Pt-Charge(O₂)/|e|	0.180	**0.184**	0.231	0.090	**0.191**	0.252
ads-Charge(O₂)/|e|	-0.160	**-0.165**	-0.178	-0.163	**-0.185**	-0.204
E_b(O₂)/eV	-1.056	**-1.342**	-1.650	-1.608	**-1.861**	-2.854
Energy Barrier/eV	1.898	**1.816**	1.320	1.593	**1.579**	1.292
Pt-Charge(CO+O₂)/|e|	0.144	**0.148**	0.207	0.110	**0.151**	0.265
ads-Charge(CO+O₂)/|e|	-0.022	**-0.088**	-0.083	-0.091	**-0.142**	-0.133
E_b(CO+O₂)/eV	-2.649	**-2.879**	-3.079	-2.850	**-3.206**	-4.303
Energy Barrier/eV	0.743	**0.732**	0.557	1.158	**1.026**	0.195
Pt-Charge(CO+O)/|e|	0.257	**0.228**	0.297	0.194	**0.301**	0.450
ads-Charge(CO+O)/|e|	-0.130	**-0.210**	-0.356	-0.220	**-0.206**	-0.337
E_b(CO+O)/eV	-1.861	**-2.200**	-2.511	-2.367	**-2.590**	-3.760
Energy Barrier/eV	0.632	**0.625**	0.469	0.710	**0.422**	0.300

Table S4. Calculated binding energies (E_b) and diffusion barriers (most favorable path) of Pt single atoms on the edges of Gr/N_1Gr/NGr supports, the corresponding CO oxidation barriers (rate-determining step), and their energy differences (ΔE).

	Pt/Gr-	Pt/N₁Gr-	Pt/NGr-	Pt/Gr-	Pt/N₁Gr-	Pt/NGr-
E_b(Pt)/eV	-5.930	**-4.619**	-4.301	-6.761	**-4.484**	-3.343
Diffusion Barrier/eV	1.489	**0.759**	0.908	1.333	**0.014**	0.519
CO oxidation	0.743	**0.732**	0.557	1.158	**1.026**	0.300
ΔE/eV	0.746	**0.027**	0.351	0.175	**-1.012**	0.219

10. The Activity of SACs on Perfect/Modified Gr/Gr-like Supports for CO Oxidation Reactions.

Table S5. The energy barriers (rate-determining step) of SACs on perfect/modified Gr/Gr-like supports for CO oxidation reactions, and their corresponding energy differences (ΔE). $\Delta E = E(Perfect) - E(Modified)$.

Influence Factor	Energy-barrier (Perfect-surface)	Energy-barrier (Modified-surface)	Energy-difference (ΔE)
Edge-effect	1.21 eV	**0.30 eV**	0.91 eV
N-doping-edge	1.16 eV	**0.30 eV**	0.86 eV
N-doping-surface	0.91 eV	1.06 eV	-0.15 eV
C-Defect [17]	1.03 eV	0.58 eV	0.45 eV
Surface-oxidation [18]	1.19 eV	0.58 eV	0.61 eV
Metal-varying [19]	3.94 eV	0.56 eV	**3.38 eV**

For edge-effect, **Perfect-surface** represents the Pt binding on the surface of NGr, and *Modified-surface* represents the Pt binding on the zigzag edge of NGr.

For metal-varying, **Perfect-surface** represents the metal (Ru) with highest energy barrier, and **Modified-surface** represents the metal (Pt) with lowest energy barrier.[19]

For different influence factors (including edge-effect, N-doping-edge, N-doping-surface, C-defect, surface oxidation), the metal for SACs all select the Pt.

References

1. G. Kresse and J. Furthmüller, *Phys. Rev. B*, 1996, **54**, 11169.

2. J. P. Perdew, K. Burke and M. Ernzerhof, *Phys. Rev. Lett.*, 1996, **77**, 3865.

3. P. E. Blöchl, *Phys. Rev. B*, 1994, **50**, 17953.

4. G. Kresse and D. Jouber, *Phys. Rev. B*, 1999, **59**, 1758.

5. O. Bengone, M. Alouani, P. E. Blöchl and J. Hugel, *Phys. Rev. B*, 2000, **62**, 16392.

6. S. Grimme, *J. Comput. Chem.*, 2006, **27**, 1787.

7. I. Fampiou and A. Ramasubramaniam, *J. Phys. Chem. C*, 2015, **119**, 8703.

8. S. Liu and S. Huang, *Carbon*, 2017, **115**, 11.

9. T. A. Manz and N. G. Limas, *RSC Adv.*, 2016, **6**, 47771.

10. N. G. Limas and T. A. Manz, *RSC Adv.*, 2016, **6**, 45727.

11. Y. Wang, et al., *Nat. Commun.*, 2019, **10**, 1506.

12. W. Sun, et al., *Nat. Mater.*, 2019, **18**, 732.

13. X. Wang, G. Zhang, Z. Wang, L. Yang, X. Li, J. Jiang and Y. Luo, *Carbon*, 2019, **143**, 700.

14. G. Mills, H. Jonsson and G. K. Schenter, *Surf. Sci.*, 1995, **324**, 305.

15. G. Henkelman, B. P. Uberuaga and H. Jónsson, *J. Chem. Phys.*, 2000, **113**, 9901.

16. D. A. Bulushev, M. Zacharska, A. S. Lisitsyn, O. Y. Podyacheva, F. S. Hage, Q. M. Ramasse, U. Bangert and L. G. Bulusheva, *ACS Catal.*, 2016, **6**, 3442.

17. Y. Tang, Z. Yang and X. Dai. *Phys. Chem. Chem. Phys.*, 2012, **14**, 16566.

18. C. Jia, Y. Zhang, X. Wang, W. Zhong, O. V. Prezhdo, Y. Luo and J. Jiang. *J. Mater. Chem. A*, 2020, **8**, 12485.

19. T. Kropp and M. Mavrikakis. *ACS Catal.*, 2019, **9**, 6864.